Smart Structures and Systems, Vol. 8, No. 1 (2011) 139-155
DOI: http://dx.doi.org/10.12989/sss.2011.8.1.139

A wireless impedance analyzer for automated tomographic mapping of a nanoengineered sensing skin

Sukhoon Pyo[1], Kenneth J. Loh[2], Tsung-Chin Hou[3], Erik Jarva[4] and Jerome P. Lynch*[1,4]

[1]*Dept. of Civil & Environmental Engineering, University of Michigan, Ann Arbor, MI 48109, USA*
[2]*Dept. of Civil & Environmental Engineering, University of California, Davis, CA 95616, USA*
[3]*Dept. of Civil Engineering, National Cheng Kung University(NCKU), Tainan, Taiwan*
[4]*Dept. of Electrical Engineering & Computer Science, University of Michigan, Ann Arbor, MI 48109, USA*

(Received September 1, 2010, Accepted November 28, 2010)

Abstract. Polymeric thin-film assemblies whose bulk electrical conductivity and mechanical performance have been enhanced by single-walled carbon nanotubes are proposed for measuring strain and corrosion activity in metallic structural systems. Similar to the dermatological system found in animals, the proposed self-sensing thin-film assembly supports spatial strain and *pH* sensing via localized changes in electrical conductivity. Specifically, electrical impedance tomography (*EIT*) is used to create detailed mappings of film conductivity over its complete surface area using electrical measurements taken at the film boundary. While *EIT* is a powerful means of mapping the sensing skin's spatial response, it requires a data acquisition system capable of taking electrical impedance measurements on a large number of electrodes. A low-cost wireless impedance analyzer is proposed to fully automate *EIT* data acquisition. The key attribute of the device is a flexible sinusoidal waveform generator capable of generating regulated current signals with frequencies from near-*DC* to 20 MHz. Furthermore, a multiplexed sensing interface offers 32 addressable channels from which voltage measurements can be made. A wireless interface is included to eliminate the cumbersome wiring often required for data acquisition in a structure. The functionality of the wireless impedance analyzer is illustrated on an experimental setup with the system used for automated acquisition of electrical impedance measurements taken on the boundary of a bio-inspired sensing skin recently proposed for structural health monitoring.

Keywords: structural health monitoring; sensing skin; wireless sensor; carbon nanotube; bio-inspired sensing; impedance tomography.

1. Introduction

The United States bridge inventory is rapidly aging with 20% of the nation's bridges currently exceeding their intended 50-year design lives; within the next 15 years, it is estimated this number will exceed 50% (AASHTO 2008). Structural aging is followed by deterioration and the need for more vigilant structural management. In addition to bridges, many other critical infrastructure systems are also rapidly aging with significant deterioration reported (ASCE 2009). Current structural health management methods are based on visual inspection with the inspector looking for visual cues that may indicate structural distress. While visual inspection is the primary tool for assessing the health of many complex structural systems such as aircrafts (Melloy *et al.* 2000), ships (Hess 2007), and

*Corresponding Author, Associate Professor, E-mail: jerlynch@umich.edu

bridges (Rolander *et al.* 2001), such methods are known to suffer from a number of limitations. Specifically, visual inspection is labor-intensive and can be highly subjective (Moore *et al.* 2001). To overcome these limitations, researchers in the field of structural health monitoring (*SHM*) are developing methods for the autonomous identification of deterioration and damage in structural systems using permanently installed sensing systems.

Within the *SHM* field, a particular emphasis has been placed on the development of new sensors that offer lower costs, reduced form factors, and greater functionality. Among the many technological developments in the realm of sensors, most notable are the new materials developed for sensing and actuating structures. In particular, piezoelectric transducers such as lead zirconate titanate (*PZT*) have been extensively studied for *SHM* applications due to their ability to be used as a sensor or actuator (Park *et al.* 2003). For example, the electro-mechanical impedance of a *PZT* patch mounted to a host structure can be used to detect structural damage. The basic concept of the impedance-based method is that damage in a structure could be detected by monitoring structural impedance in a local area using high-frequency vibration (Peairs *et al.* 2004). Alternative *SHM* approaches based on the controlled introduction of high-frequency elastic stress waves in thin plate structural elements (i.e., Lamb waves) have also been illustrated using *PZT* pads (Sohn and Kim 2010). In addition to successful results derived in the laboratory, *PZT*-based sensing for *SHM* is also beginning to find its way to practical settings. For example, *PZT*-based active damage detection techniques for nondestructive evaluation of operational steel bridges have been reported (Park *et al.* 2006).

Other engineered materials under development for *SHM* include multifunctional, self-sensing materials that possess electrical properties that are linked to the mechanical and physical properties of the material (Dharap *et al.* 2004, Loh and Chang 2010, Loh *et al.* 2007). Among the many multifunctional materials under development, carbon nanotube composites have garnered significant research attention in recent years. Single- and multi-walled carbon nanotubes (*SWNT* and *MWNT*, respectively) have been first reported in the literature by (Iijima 1991). Due to their impressive mechanical and physical properties (e.g., high tensile strength, high elastic modulus, and large surface area), the *SHM* community has explored the inclusion of *SWNTs* in polymer matrices to create conformable thin-film sensors for measuring strain (Dharap *et al*. 2004) and *pH* (Loh *et al.* 2007). The inclusion of *SWNTs* in the polymer matrix modifies the bulk conductivity of the composite while simultaneously reinforcing the composite to achieve high tensile strength and stiffness (Loh *et al*. 2009b).

A distinct advantage of multifunctional materials used for sensing within *SHM* systems is their ability to essentially achieve a sensor measurement everywhere the material is. This creates the opportunity to deviate from the traditional point-based sensing strategies universally used in *SHM* systems (i.e., the use of sensors that take localized measurements at a specific point in the structure). Similar to dermatological systems found in animals, an engineered "sensing skin" possessing transduction mechanisms throughout its area and deposited on the surface of a structure can serve as a platform for spatial structural sensing. Using a controlled electrical stimulation and a corresponding set of voltage measurements taken at the skin boundary, two-dimensional (2D) maps of the skin's electrical conductivity can be derived through the use of the electrical impedance tomography (*EIT*) technique (Hou *et al*. 2007). Since thin film conductivity is calibrated to an applied external stimulus such as strain or *pH*, conductivity mapping by *EIT* will yield a corresponding 2D structural damage map (Loh *et al.* 2009). However, due to the complexity of the inverse-problem that *EIT* solves, the data acquisition requirements of *EIT* can be challenging to achieve. Specifically, *EIT* requires a large number of electrodes mounted to the boundary of the skin, precise control of the direct and alternating current (*DC* and *AC*, respectively) excitation, and repeated injection of electrical current

on many different electrode pairs (Holder 2005).

A powerful but low-cost approach to *EIT* data acquisition is proposed herein for bio-inspired thin-film sensing skins. A wireless impedance analyzer is designed such that any of its 32 channels can output an electrical current with a user-prescribed frequency, mean, and amplitude, while the remaining multiplexed channels can measure boundary voltage using an onboard analog-to-digital converter. Upon data acquisition, an onboard microcontroller provides ample computational resources for calculating electrical impedance (a complex-valued material property) from the input/output electrical measurements. Finally, a wireless transceiver is integrated to free the system from its dependence on coaxial wiring for the communication of electrical impedance data. This portable, low-cost wireless impedance analyzer is unique in its design when compared to other wireless impedance analyzers previously proposed for *PZT*-based *SHM* (Mascarenas *et al.* 2007, Park *et al.* 2009). First, the analyzer proposed in this study supports a large number of channels that are necessary for *EIT*; in contrast, previously proposed wireless impedance analyzers have a limited number of channels (e.g., eight or fewer channels). The wireless impedance analyzer in this study also has a flexible current generation unit not found in other systems that have relied on a commercial impedance measurement integrated circuit (i.e., Analog Devices AD5933). The current generation unit used in the proposed wireless impedance analyzer allows the user to define the electrical current, whereas analyzers based on the AD5933 hide this functionality from the user and only reports measured electrical impedance.

This paper begins with an overview of the fabrication and electromechanical characterization of bio-inspired sensing skins. As mentioned earlier, the sensing skin is a thin conformable film assembled at the nano-scale using single-walled carbon nanotubes and polyelectrolyte (*PE*) species. Similar to skin found in living animals, the thin film can be designed to sense mechanical (i.e., strain) and chemical (i.e., corrosion) stimuli in a distributed fashion. Second, the hardware design of the wireless 32-channel impedance analyzer is presented, including a description of its sensing interface, computational core, and wireless transceiver. Then, the wireless impedance analyzer is validated for its ability to interrogate and map the spatial conductivity of *SWNT-PE* thin films deposited onto the surface of a steel structure. Specifically, the wireless impedance analyzer will capture the changes in film conductivity when corrosion occurs in the vicinity of film penetrations and tears. Finally, the paper concludes with a summary of the key findings and results.

2. Bio-inspired thin-film sensing skin for *SHM*

Skin is the largest human organ with a cellular design optimized to protect underlying tissue from the environment (Wilkinson 1998). In particular, skin is a multilayered system consisting of an outer epidermis layer, a thick inner dermis layer, and a subcutaneous layer. The outer epidermal layer is comprised of dead cells that are waterproof and designed to be mechanically robust to friction, tension, and shear. The dermis layer beneath is a sophisticated multi-layered system with a dense network of neural receptors that provide the skin with its sensing ability. Different receptor types exist within the dermis neural network to sense touch, temperature, and pain. Human skin is an ideal basis for bio-inspiration of new *SHM* sensing technologies for many reasons. First, skin is an impressive natural multifunctional material system optimized to offer incredible strength (to keep germs out of the body) while providing distributed sensing capabilities. The intricate neural network contained within the structure of the skin allows animals to detect the precise location and magnitude of

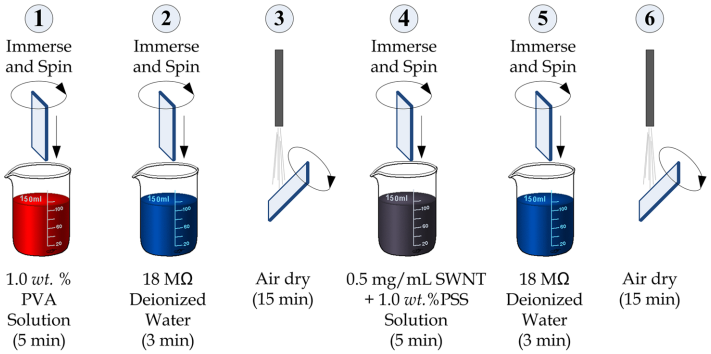

Fig. 1 *LbL* assembly of one bi-layer of the $(SWNT\text{-}PSS/PVA)_{50}$ sensing skin

stimuli (e.g., touch, heat) in real-time.

A bio-inspired skin system is proposed as a self-sensing coating for metallic structures. The objective of the sensing skin is to sense the response (i.e., strain) and deterioration (i.e., corrosion) of the underlying structural system upon which it is placed. Like all natural systems, skin is naturally fabricated based on a spontaneous self-assembly process that begins at the atomistic scale (Nagayama 1997). For example, nature begins its assembly process with amino acids, which are small molecular structures that nature uses to assemble proteins. Protein molecules are then used to assemble sub-cellular components (e.g., organelles) that in turn are used to assemble cells. Cells then self-organize, reproduce, and form organs and other macro-scale functional elements that are found in all living beings (Alberts *et al.* 2008). This self-assembly process is inherently a "bottom-up" approach, which consists of assembling increasingly complex structured systems from smaller functional blocks. Adopting a similar approach to bottom-up assembly of engineered materials has become possible with many of the recent advances in nanotechnology. The controlled assembly of smaller molecular structures to form complex molecular aggregates at the nano- and micro-scales offers unprecedented opportunities to achieve desired physical, electrical, and mechanical functionalities at the macro-scale.

In this study, a directed bottom-up assembly method known as layer-by-layer (*LbL*) is explored for the fabrication of thin film molecular structures that provide functionality similar to that of human skin. *LbL* deposition is a true bottom-up assembly method where supramolecules (i.e., polyelectrolyte species) are adsorbed onto the surface of a substrate through non-covalent or covalent atomic attractions (Fig. 1). Motivation for the adoption of the *LbL* technique is due to the fact that this method is low-cost, creates highly homogenous composite materials, and does not require chemical modification of constituent materials (Decher and Schlenoff 2003). Furthermore, multi-layered thin films of varying thicknesses can be easily assembled by repeatedly depositing sets of oppositely charged mono-layers (i.e., bi-layers) (Mamedov *et al.* 2002). Specifically, *SWNT* fillers included in an *LbL*-assembled poly(vinyl alcohol) (*PVA*)/poly(sodium 4-styrenesulfonate) (*PSS*) thin film will be explored to provide a basis for distributed, multi-modal sensing of physical phenomena pertinent to structural health monitoring applications. These *LbL* thin films are referred to as $(SWNT\text{-}PSS/PVA)_n$, where n is the number of bi-layers fabricated.

3. Electrical impedance tomographic mapping

The conductivity of $(SWNT\text{-}PSS/PVA)_n$ thin films have been shown to vary as a function of strain

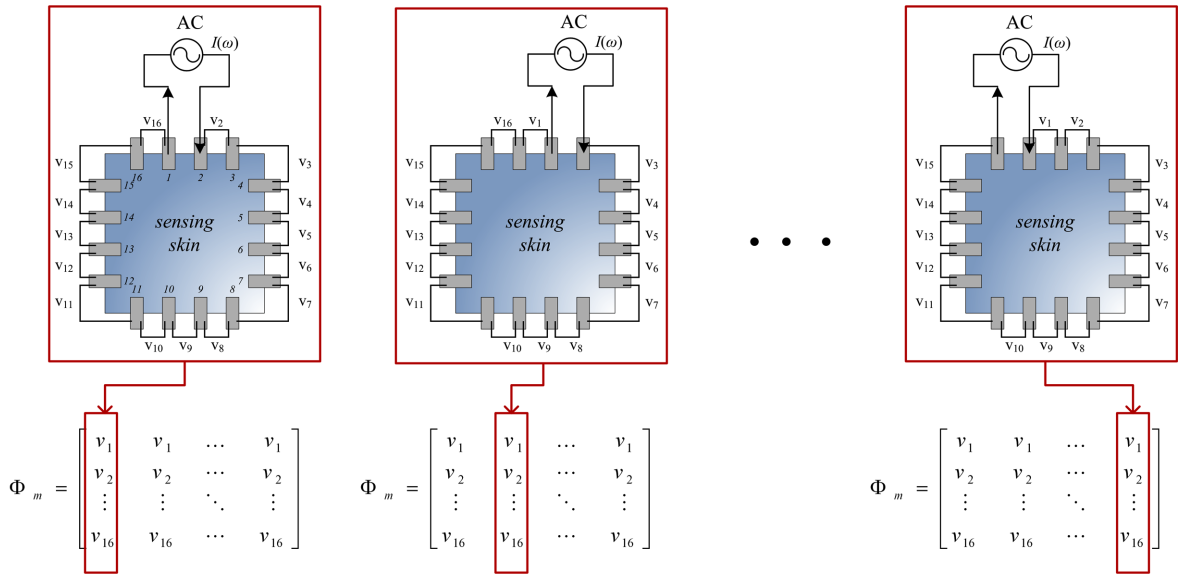

Fig. 2 *EIT* data acquisition consists of moving the point of current injection around the thin film boundary with boundary voltages measured. Each instance of current injection represents one column of the boundary electric potential matrix used in the *EIT* analysis

(Loh *et al.* 2007, Loh *et al.* 2008). This self-sensing attribute of the fabricated thin film can be leveraged to create strain sensors for *SHM* applications. However, if the conductivity of the entire thin film can be mapped, then the film can be utilized as a distributed sensor platform (i.e., sensing skin) that provides a spatial mapping of strain. To this end, electrical impedance tomography is adopted to provide a spatial mapping of sensing skin conductivity based on electrical measurements taken at the skin boundary. The application of *EIT* to determine changes in sensing skin spatial conductivity to strain, pH, and tears has been successfully demonstrated in previous studies (Hou *et al*. 2007, Loh *et al.* 2009a).

EIT begins with an analytical model of the flow of electricity in a body (e.g., a multifunctional thin film) based on an input signal or the injection of a controlled current (either *DC* or *AC*) at two points on the body boundary (Fig. 2). In general, a finite element method (*FEM*) model describing electrical flow in the body is formulated from the Laplace vector equation. In the forward problem, the distribution of body conductivity is known and the analytical model is used to predict the output electrical potential (i.e., voltage) on the boundary of the body due to the applied current. In contrast, *EIT* is an inverse problem in which the distribution of conductivity is unknown and is solved for using the known input (i.e., injected current) and output (i.e., the boundary electrical potential). Under one instance of current injection, the current-voltage data set is not sufficient for solving the underdetermined inverse problem (Holder 2005). Rather, a redundant set of input-output data is necessary to render the *EIT* problem tractable. Hence, *EIT* necessitates stimulation of the body at multiple locations along the body boundary with corresponding electrical potential measured for each unique current injection.

The general state-of-practice is to divide the boundary of the body into an equal number of segments with an electrode placed at the center of each segment. As shown in Fig. 2, the thin film has 16 electrodes placed equidistantly with four electrodes mounted on each side of the square film.

The electrodes are numbered 1 through 16 as shown. First, the current is injected on the 1-2 electrode pair as illustrated in Fig. 2. If the injected current is a *DC* current, then the electric potentials, *v*, are measured on all of the boundary electrode pairs as shown in Fig. 2. If the injected current is an *AC* current, then the voltage amplitude and lag (relative to the *AC* current) are measured. The measured electric potentials make up the first column of the electric potential matrix, Φ. Next, the current is applied to the 2-3 electrode pair with the boundary electric potential again measured. The measured potentials consist of the second column of the electric potential matrix, Φ. This process repeats until all adjacent electrode pairs have been used to stimulate the thin film. If done manually, this process can be extremely time-consuming, thereby ruling out the possibility of employing the sensing skin as an autonomous, real-time *SHM* system. Therefore, a portable wireless impedance analyzer is proposed to fully automate *EIT* data collection in the field setting.

4. Wireless impedance analyzer for sensing skin interrogation

A low-cost wireless impedance analyzer is designed for automated impedance measurements and acquisition of *EIT* data (Fig. 3). The device is designed with a single, high-precision current source offering impressive control over the generated current's amplitude and frequency. A versatile multiplexor interface is integrated with the wireless impedance analyzer to offer 32 independently addressable channels to which the current can be injected and sensing skin boundary potential can be simultaneously measured. At the core of the device is a low-power 8-bit microcontroller that operates the device and measures the boundary electric potential using its internal 10-bit analog-to-digital converter (*ADC*). In addition, a wireless transceiver is integrated with the data acquisition package to offer untethered communication with other wireless sensors within a structure's *SHM* system. The wireless impedance analyzer is fabricated using four separate printed circuit boards (*PCB*) with the boards connected using interlocking headers and flat flexible cables (*FFC*). Each board is based on a specific task within the *EIT* data acquisition process. The four *PCBs* are termed the microcontroller, direct digital synthesizer (*DDS*), multiplexor and wireless transceiver boards.

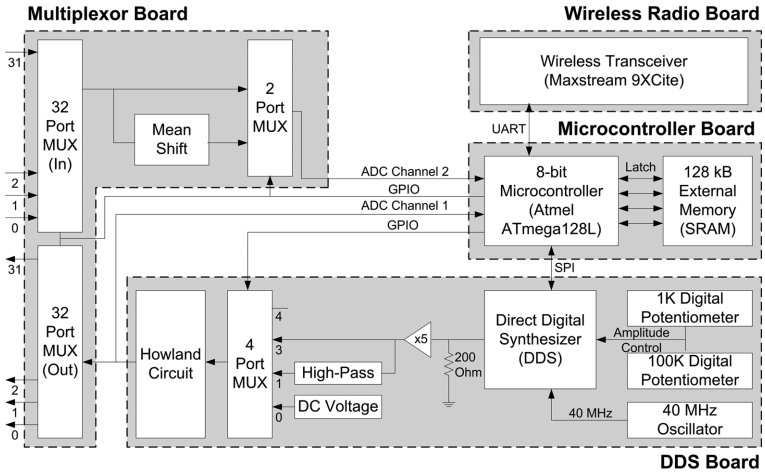

Fig. 3 Architectural overview of the proposed wireless impedance analyzer supporting 32 data acquisition channels

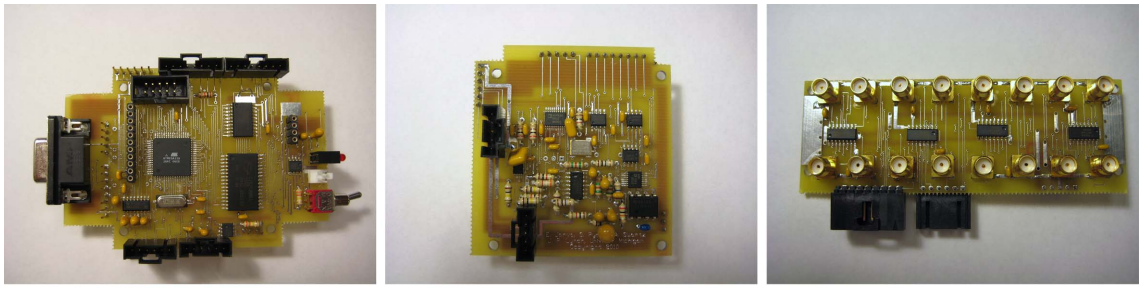

Fig. 4 Individual components of the wireless impedance analyzer: (a) microcontroller board, (b) *DDS* board and (c) multiplexor board

4.1 Microcontroller board

The microcontroller board (Fig. 4(a)) is a critical element of the wireless impedance analyzer because it is primarily responsible for the entire unit's operation. At the core of the microcontroller board is a low-power 8-bit microcontroller (Atmel ATmega128) that is powered by a regulated 5 V power supply. The 5 V power supply regulates its output based on the battery power provided to the unit (7.5 V or higher). An 8 MHz crystal is included in the microcontroller board to provide a clock signal to the microcontroller. Internal to the microcontroller is 128 kB of read-only flash memory; this memory is for the storage of software used to operate the microcontroller. An additional 128 kB of static random access memory (*SRAM*) is included in the microcontroller board design to provide memory for data storage. The peripheral services of the microcontroller are used to interface with the other circuit components, including the wireless transceiver (using the universal asynchronous receiver transmitter, or *UART*) and the variety of multiplexors (*MUX*) on the direct digital synthesizer board and multiplexor board. The internal 10-bit *ADC* of the microcontroller is used to collect voltage waveforms generated by the multiplexor board. The input voltage range of the microcontroller *ADC* is 0 to 5 V.

4.2 Direct digital synthesizer (DDS) board

The direct digital synthesizer (*DDS*) board (Fig. 4(b)) is primarily responsible for the generation of the electrical stimulus, that is applied to the sensing skin. As such, it is where the current is generated and regulated by the microcontroller for output by the multiplexor board. The main component of the *DDS* board is the Analog Devices AD9834 direct digital synthesizer capable of outputting sinusoidal signals at frequencies as large as 75 MHz. A 40 MHz oscillator is included on the *DDS* board to provide a clock signal to the AD9834 *DDS*. The *DDS* board is controlled by the microcontroller (i.e., Atmel ATmega128) with the microcontroller communicating desired frequencies and phase shifts to the *DDS* via a serial peripheral interface (SPI). Using a 40 MHz reference oscillator, the *DDS* board is capable of outputting sinusoidal signals with frequencies between 0.15 Hz and 20 MHz in 0.15 Hz increments. The output signal from the AD9834, when passed over a 200 Ω resistor to ground, can generate a sinusoidal voltage between 30 to 600 mV. The actual peak-to-peak amplitudes of the generated sinusoidal signal are defined by two digital potentiometers integrated with the *DDS* board that are controlled by the microcontroller. To amplify the output signal, a non-

inverting amplifier is designed using standard operational amplifiers to amplify the AD9834 signal by a factor of five.

To offer the end-user of the wireless impedance analyzer maximum flexibility, the electrical signal generated by the *DDS* is split into two parts. First, the sinusoidal signal whose peak-to-peak span is between 30 to 600 mV (i.e., non-zero mean) is passed to one channel of a 4-channel multiplexor. The other part of the split is passed through a high-pass filter to remove the non-zero mean. This high-passed signal is then fed to the second channel of the multiplexor. Finally, a constant voltage is generated by dividing the 5 V reference of the *DDS* board using a digital potentiometer for generating a user-selected voltage that is between 0 and 5 V. This *DC* voltage is then passed to the third channel of the multiplexor. The microcontroller is capable of using its general purpose input/output pins to select which of the three outputs to use (i.e., *AC* signal with non-zero mean, *AC* signal with zero mean, and *DC* signal). The output of the multiplexor is then fed to a standard Howland voltage-current converter for output by the *DDS* board. The maximum permissible current amplitude capable by the converter is ±5 mA. The output of the Howland circuit is also fed to the microcontroller *ADC* and sampled using the *ADC*'s first input channel.

4.3 Multiplexor board

The multiplexor board is used to output the *DDS* board's regulated *AC* or *DC* current while simultaneously recording the corresponding voltage response of the sensing skin (Fig. 4(c)). To ensure the wireless impedance analyzer can be used for electrical impedance tomography, a large number of input/output channels are desired. The multiplexor board includes 16 gold plated subminiature version A (*SMA*) jacks to which coaxial wires (i.e., electrodes) can be attached. Internally, the multiplexer board includes four 8-channel multiplexing integrated circuit chips. Two of the 8-channel multiplexors are used to route the *DDS* current to any of the board's 16 electrodes as selected by the microcontroller using the multiplexors' select bits. The other two multiplexors are used to feed the 16 electrode connections to the microcontroller's 10-bit *ADC* for sampling. Again, select bits on the multiplexors are used by the microcontroller to select which electrode it will collect data from using its *ADC*. The voltage signal from the multiplexor board is input to the second input channel of the *ADC*. If the sensing skin is stimulated by the *DDS* board with non-zero mean *AC* or *DC* inputs, the recorded voltages will fall within the *ADC*'s 0 to 5 V input range. However, if the zero mean *AC* input is applied to the sensing skin, the voltage generated by the sensing skin will also have a zero mean. Hence, a voltage mean shift is performed on the multiplexor board to place the mean of the measured voltage to 2.5 V which falls in the middle of the *ADC* input voltage range. Using the applied *DDS* current as measured on the first *ADC* channel and electrode voltages measured on the second *ADC* channel, the microcontroller can calculate the sensing skin's impedance based on amplitude measurements and the relative phase shift between the *AC* current and measured voltage.

4.4 Fully assembled device

The microcontroller board includes a set of header pins to accommodate the attachment of the wireless transceiver that is on its own board (i.e., wireless radio board). The wireless transceiver is a commercial radio: Maxstream 9XCite digital transceiver. The 9XCite radio operates on the 900 MHz radio band and is capable of data rates as high as 38.4 kbps and a line-of-sight communication

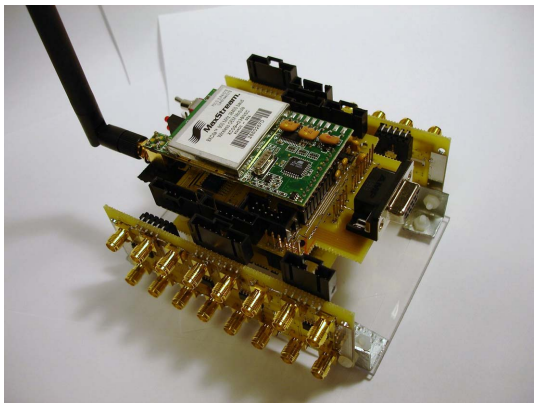

Fig. 5 Fully assembled wireless impedance analyzer prototype

range of 300 m. The radio is controlled by the microcontroller through a standard *UART* interface. The wireless transceiver is connected to the top-side of the microcontroller board. The microcontroller board is then attached to the *DDS* board using a set of header pins included in the *DDS* board design. The multiplexor board is attached to the microcontroller board using flat flexible cables. A unique feature of the design of the wireless impedance analyzer is that multiple multiplexor boards can be included in the assembled device to increase the number of channels. In this study, two multiplexor boards (16 channels each) are integrated with the wireless impedance analyzer to accommodate a total of 32 electrodes. The wireless impedance analyzer, when fully assembled (Fig. 5), is 10 cm long, 6 cm wide and 5 cm tall. The device can be powered by standard *AC* power available from a standard electrical outlet or can be powered by a 7.5 V battery pack constructed from five AA batteries.

5. Validation of the wireless impedance analyzer

Two validation experiments are performed to verify the accuracy and reliability of the proposed wireless impedance analyzer. In the first, the output of the *DDS* board is analyzed to ensure it is capable of outputting *AC* currents with precise amplitudes. The generated *AC* current is applied to a 1200 Ω resistor, and the corresponding voltage is measured (Fig. 6(a)). In the second, electrical impedance spectroscopy (*EIS*) is conducted on a resistor-capacitor (RC) circuit using a four-point probe method (Fig. 6(b)). The *EIS* test will analyze the ability of the wireless impedance analyzer to output an *AC* current of varying frequency, capture the circuit voltage, and calculate complex-valued impedance.

5.1 Assessment of DDS board output

The *DDS* output of the wireless impedance analyzer is analyzed by generating an *AC* current applied to a 1.2 kΩ resistor as shown in Fig. 6(a). The amplitude of the *DDS* board is configured to be 1 mA peak-to-peak with a non-zero mean. A separate Agilent data acquisition system is attached to the two terminals of the 1.2 kΩ resistor to record the resistor voltage at a 600 Hz sample rate. Using Ohm's Law, the current can be calculated based on the measured voltage. The measured

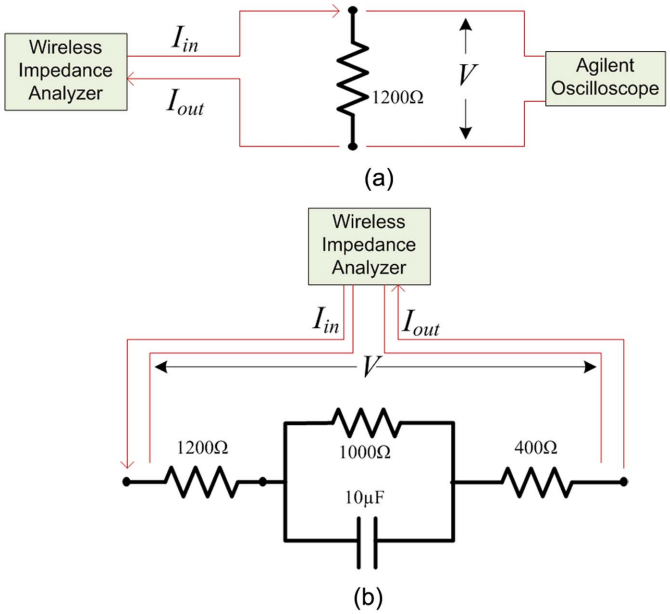

Fig. 6 Validation experiments: (a) assessment of wireless impedance analyzer *DDS* output using a 1.2 kΩ resistor and (b) RC circuit for electrical impedance spectroscopy

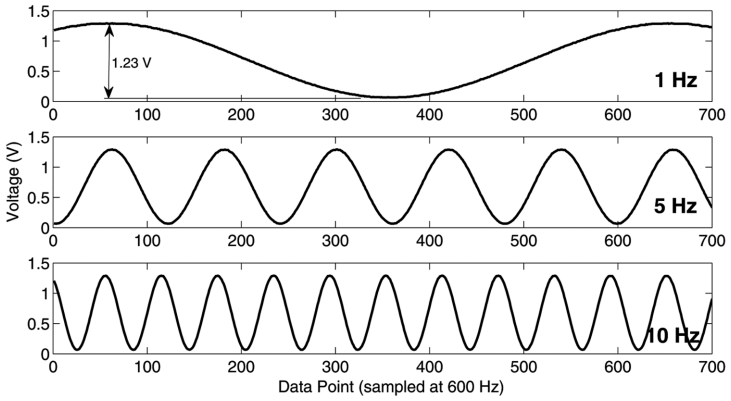

Fig. 7 Measured voltage across the 1.2 kΩ resistor due to the applied 1 mA peak-to-peak amplitude *AC* signal using three different frequencies: 1 (top), 5 (middle) and 10 Hz (bottom)

voltage signals corresponding to three different *AC* frequencies (1, 5, and 10 Hz) are shown in Fig. 7. As shown, the peak-to-peak voltage across the 1.2 kΩ resistor is 1.23 V and corresponds to 1.025 mA according to Ohm's Law. Furthermore, the *AC* frequencies are also measured from the voltage time histories to be that desired: 1, 5, and 10 Hz.

5.2 Electrical impedance spectroscopy (EIS)

After verifying the accuracy of the *DDS* board, the ability of the wireless impedance analyzer to output *AC* currents of varying frequency and to simultaneously record voltage is assessed. Specifically, electrical impedance spectroscopy is performed on the *RC* circuit shown in Fig. 6(b). The wireless

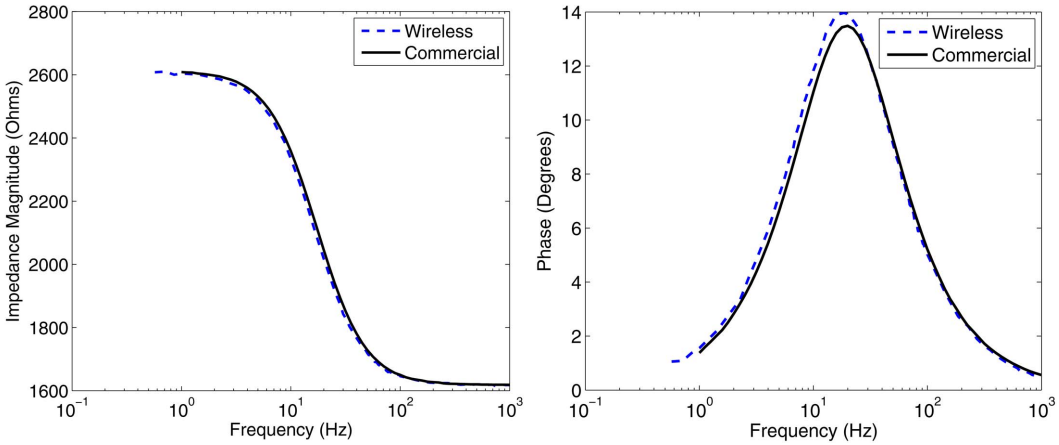

Fig. 8 Electrical impedance spectroscopy of an *RC* circuit as measured by the wireless impedance analyzer: (left) impedance magnitude and (right) impedance phase

impedance analyzer is configured to automatically apply a zero-mean *AC* signal (0.5 mA amplitude) with a frequency varying from 0.75 to 1000 Hz in increments of 0.15 Hz. At each frequency, the microcontroller board records both the applied *AC* signal and the corresponding voltage waveform. Using the peak amplitude of the measured voltage and the phase shift in the measured voltage relative to the *AC* current input, the impedance of the circuit is wirelessly transmitted by the wireless impedance analyzer. To verify the electrical impedance data collected by the prototype, the results are compared to impedance measurements taken by a commercial impedance analyzer (Solartron 1260 impedance-gain/phase analyzer) during an independent test on the same test circuit. Fig. 8 shows that the results obtained by the prototype wireless impedance analyzer and the commercial impedance analyzer are in strong agreement. The impedance amplitudes are in perfect agreement with errors less than 1% between the wireless and commercial impedance analyzers. However, some minor disagreement in the impedance phase is identified with the wireless impedance analyzer error bounded by 4%. The inaccuracy in phase is attributed to minor parasitic capacitance within the unit's circuit design. While this capacitance can be eliminated in future device improvements, it can also be calculated and easily removed from the impedance measurements.

6. Corrosion assessment by *EIT* of the bio-inspired sensing skin

Most metallic structures that operate in harsh environments (e.g., aircraft, bridges, pipelines) are coated with sophisticated coating systems to prevent corrosion to the underlying metallic surface. For example, primers and corrosion-inhibiting layers are common within structural coating systems. While such systems have been proven effective, they are only effective if the coating itself remains undamaged. When the coating system is nicked or cut, the metallic surface is exposed and corrosion can occur. Assuming the aforementioned *SWNT-PE* thin film assembly is included in such a coating system for monitoring structural strain and cracking (Loh *et al*. 2009a), this study explores the corrosion process that can occur on the metallic structural surface when openings in the sensing skin exists. Electrical impedance tomography is performed to analyze the process of corrosion formation within an accelerated corrosion test configuration.

6.1 Experimental details

A carbon steel plate (25 mm wide, 55 mm long, 1.2 mm thick) is selected to serve as the substrate for the *LbL* assembly of the *SWNT-PSS/PVA* thin film. First, the surface of the carbon steel plate is treated with acetone and ethyl alcohol to rid its surface of impurities and oil. Second, the steel plate is coated with a thin coat of primer (Krypton General Purpose Primer) to ensure the underlying steel is electrically isolated from the *SWNT-PE* thin film assembly. After the primer has been permitted time to properly dry (72 hr), the *LbL* process is initiated to form a 50 bi-layer thin film ($(SWNT\text{-}PSS/PVA)_{50}$). Upon film fabrication, eight conductive electrodes are formed along each side of the film boundary to form a total of 32 electrodes for the entire film. Each electrode is a thin slice of copper tape bonded to the sensing skin surface by silver paste. Once the silver paste on the electrodes has dried, the film and primer are mechanically etched on one side of the specimen to expose two 7 mm circular regions of the bare carbon steel substrate. Finally, a plastic well is then secured over the exposed circular holes using high-vacuum grease (schematic and photograph of a specimen are shown in Fig. 9. A coaxial wire is attached to each electrode using an alligator clip with each of the 32 coaxial wires terminated at the impedance analyzer multiplexor board. The coaxial cables contain an inner signal line and a grounded sheath that prevents noise from affecting the signals transmitted over the cable.

Accelerated corrosion of the exposed carbon steel region is conducted by pipetting into plastic wells #1 and #2 (as denoted in Fig. 9(a)) 0.1 M and 1.0 M sodium chloride solutions, respectively. These plastic wells are used to confine salt solutions to the selectively etched areas and to promote corrosion and rust formation at the two circular regions; the plastic wells also serve to prevent the solutions from wetting other regions of the film. It is known that corrosion of steel occurs due to the oxidation of iron (within the steel) to form iron oxide (i.e., rust) (Ahmad 2003)

$$3Fe + 4H_2O \rightarrow Fe_3O_4 + 8H^+ + 8e^- \tag{1a}$$

$$2Fe + 3H_2O \rightarrow Fe_2O_3 + 6H^+ + 6e^- \tag{1b}$$

When water is available for the oxidation of iron, the reaction kinetics highly favors the formation of iron oxide. As a result, with increased water exposure time, rust will continue to form as long as the

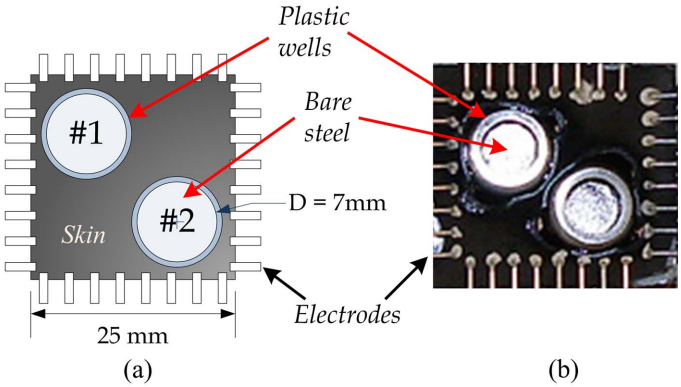

Fig. 9 (a) Schematic and (b) photograph show the sensing skin deposited onto a primer-coated carbon steel substrate. Two circular regions (i.e., wells #1 and #2) are etched to expose the bare steel substrate for accelerated corrosion testing

chemical reaction is not rate-limited by iron availability.

For this validation study, the *NaCl* solutions are initially pipetted into the plastic wells for 5 min (herein referred to as the "corrosion time") and subsequently removed. Then, the specimens are allowed sufficient time to dry (1 hr) prior to *EIT* spatial conductivity mapping. The *EIT* boundary potential is measured. This procedure completes one sensing skin measurement corresponding to 5 min of corrosion time. Then, fresh 0.1 M and 1.0 M *NaCl* solutions are again pipetted into the plastic wells for another 5 min; the procedure is repeated until a total corrosion time of 90 min has occurred.

6.2 Results and discussion

Upon etching the sensing skin to expose two circular regions of the bare steel substrate, an initial *EIT* spatial conductivity map is obtained to serve as the undamaged baseline. For *EIT* mapping, an *AC* current (0.1 mA) with zero mean and 100 Hz frequency is used. Then, following the experimental details previously outlined, successive time-lapsed *EIT* maps are acquired for each corrosion time to

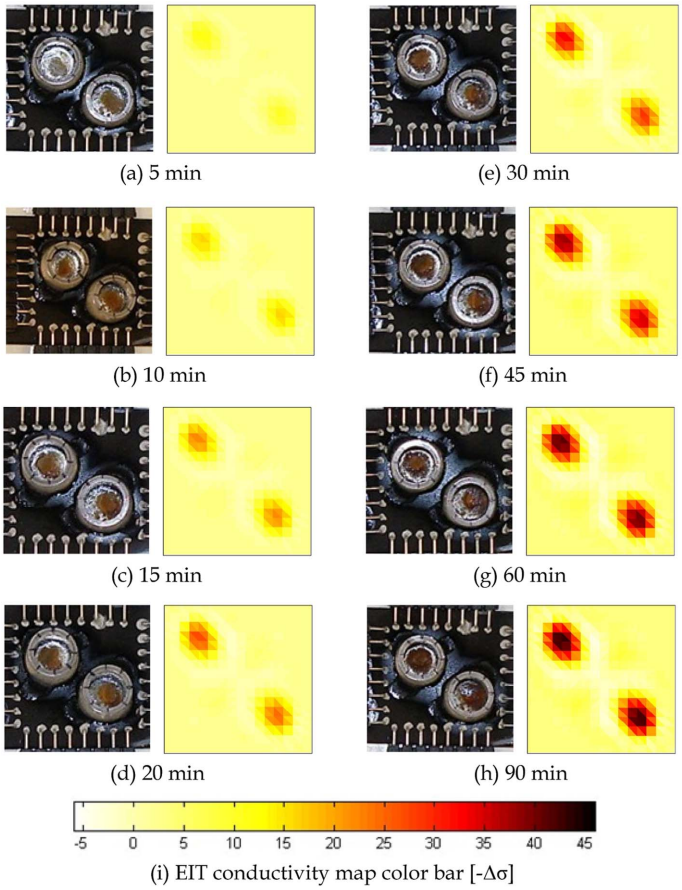

Fig. 10 (a) - (h) Set of images at certain corrosion times shows the (left) photograph of the corroded sensing skin-coated specimen as well as the (right) corresponding *EIT* spatial conductivity maps and (i) The color bar is shown as the negative change in electrical conductivity [S-cm-1]

monitor the corrosion byproduct formation that results from concentrated sodium chloride solution exposure. The actual *EIT* algorithm is performed off-line using a standard personal computer.

Fig. 10 presents the sensing skin spatial conductivity maps (i.e., relative to the baseline) and the corresponding photographs taken at various corrosion times ranging from 5 to 90 min. It can be observed that the skin's electrical conductivity in the vicinity of the wells decrease as corrosion time increases. The localized decrease in conductivity corresponds to increasing rust (or iron oxide) formation on the exposed steel surfaces, as is also confirmed by the time-lapsed photographs shown in Fig. 10. On the other hand, regions outside of the wells that have not been exposed to salt solutions remain in their pristine state (i.e., no corrosion) throughout the duration of the test. Similarly, the *EIT* spatial conductivity maps in Fig. 10 also indicate that the change in conductivity at regions outside the well are insignificant and are approximately zero. Thus, these results provide evidence that the carbon nanotube sensing skins employed in this study show potential for spatial corrosion monitoring when tears and breaks in the sensing skin occurs.

After initially removing the sensing skin and primer at the well locations, the baseline *EIT* conductivity map (i.e., pre-corrosion) reveals that the etched regions possess low electrical conductivity and is significantly less conductive than the thin film. As corrosion takes place and thin layers of electrically insulating iron oxides form on the steel substrate, the conductivity at the corroded site should decrease. This hypothesis is consistent with the experimental findings. When the average negative change in conductivity at wells #1 and #2 are plotted as a function of corrosion time, an exponential decrease in well conductivity is obtained as shown in Fig. 11. With increasing salt solution exposure time, the average negative conductivity change for both wells #1 (1.0 M *NaCl* solution) and #2 (0.1 M *NaCl* solution) follow the same trend; initially, a sudden drop in conductivity is observed, followed by a decreasing rate until it plateaus at $t = 90$ min. The plateau effect is due to the fact that the area of bare steel (or iron availability) decreases with increasing iron oxidation and rust formation. The results obtained in Fig. 11 agree with those obtained by Yonemoto and Shida (1998) where they have determined that their proposed corrosion sensor's impedance increases in a

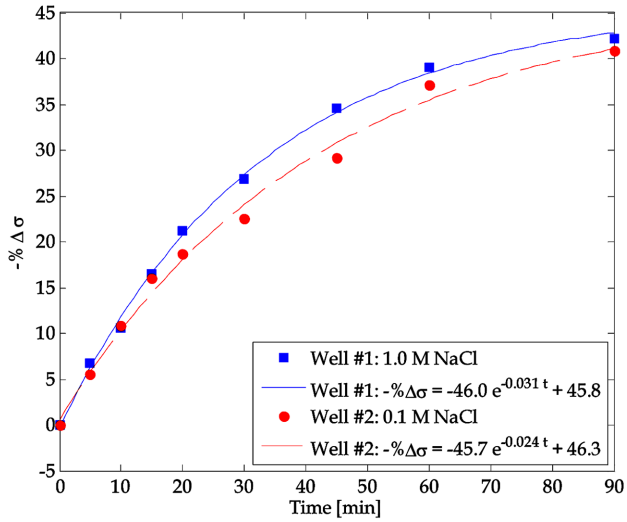

Fig. 11 The average conductivity at each well is computed and plotted as a function of corrosion time, and the results are fitted to an exponential decay model

similar fashion with increasing rust thickness. In fact, the experimental results obtained in Fig. 11 can be easily fit to an exponential decay model of the form $-\Delta\sigma=-Ae^{-Bt}+C$ via regression analysis. Results from numerical fitting suggest that the average change in thin film conductivity due to corrosion byproduct formation is well-behaved. The nanocomposite conductivity decreases at an exponential rate of 0.031 min^{-1} for well #1 (1.0 M *NaCl*) and 0.024 min^{-1} for well #2 (0.1 M *NaCl*). The faster corrosion rate for well #1 is consistent with the higher concentration of salt solution employed during testing.

7. Conclusions

In previous studies, it has already been shown that carbon nanotube-based thin films change their electrical properties in response to applied strain or pH (Hou *et al*. 2007, Loh *et al.* 2009). Unlike traditional sensors based on data measurements at a discrete point, these thin films can be employed as a distributed sensor platform (or sensing skin). Electrical impedance tomography utilizes boundary electrical measurements for mapping thin film spatial conductivity; however, due to the complexity of the *EIT* inverse problem, multiple sets of boundary current injection and potential measurements are required. Realization of a real-time and autonomous *SHM* system demands an alternative solution for rapid automated *EIT* data collection. Thus, a wireless impedance analyzer is designed and proposed for automated impedance measurements and for the acquisition of electrical impedance tomography data. Unlike other wireless impedance analyzers, the user can selectively output an electrical current of controlled amplitude and frequency (i.e., from near-*DC* to 20 MHz) at any one of its 32 independently addressable channels, while the device samples voltage at the remaining electrodes. All the measurements are controlled by a low-power 8-bit microcontroller, and its internal 10-bit *ADC* digitizes the acquired data. The data collected can be stored in an onboard 128 kB *SRAM*, but data communication to a centralized data repository is ultimately achieved with a Maxstream 9XCite wireless transceiver integrated with the device hardware. The fully assembled unit is 10 cm long, 6 cm wide, and 5 cm tall and can draw its power from an *AC* electrical source or from a 7.5V battery pack.

Upon hardware implementation, three tests have been performed to validate the wireless impedance analyzer's impedance and *EIT* data acquisition performance. First, the device is commanded to interrogate a 1.2 kΩ resistor using 1 mA *AC* current outputs at three different *AC* frequencies (1, 5, and 10 Hz), while the voltage response is measured by the wireless unit and a tethered Agilent data acquisition system. The results obtained show that the wireless impedance analyzer is capable of generating electrical signals at prescribed amplitudes and frequencies. For the second test, the wireless impedance analyzer is connected to an *RC* circuit for conducting electrical impedance spectroscopy. The device applies a zero-mean *AC* signal from 0.75 to 1000 Hz while the corresponding voltage magnitude and phase is recorded at each applied *AC* frequency for computing the impedance of the *RC* circuit. When compared to the results obtained by a commercial Solartron 1260 impedance analyzer, good agreement and low measurement errors are confirmed. Finally, electrical impedance tomography is employed for spatial conductivity mapping of a $(SWNT\text{-}PSS/PVA)_{50}$ thin film deposited onto a primer-coated steel plate. The objective is to identify localized changes in thin film conductivity when concentrated salt solutions accelerate corrosion and rust formation at exposed metallic structural surface areas. It has been shown that the *EIT* spatial conductivity maps show localized decreases in conductivity corresponding to rust (or iron oxide) formation. On the other hand, the sensing skin's conductivity remains fairly constant at other locations where there is no

corrosion activity. Thus, these results validate the use of *EIT* for mapping thin film spatial conductivity, and the wireless impedance analyzer provides a more cost effective and rapid method for *EIT* data acquisition.

Acknowledgements

This research is supported by the National Science Foundation under Grant Number CMMI-0846256 (Program Manager: Dr. S.C. Liu). The authors would also like to gratefully acknowledge additional support offered by the U.S. Department of Commerce, National Institute of Standards and Technology (NIST) Technology Innovation Program (TIP) under Cooperative Agreement Number 70NANB9H9008.

References

AASHTO. (2008), "Bridging the gap: restoring and rebuilding the nation's bridges", American Association of State Highway and Transportation Officials, Washington D.C.

Ahmad, S. (2003), "Reinforcement corrosion in concrete structures, its monitoring and service life prediction - a review", *Cement Concrete Comp*., **25**(4-5), 459-471.

Alberts, B., Johnson, A., Lewis, J., Raff, M., Roberts, K. and Walter, P. (2008), Molecular Biology of the Cell, Garland Science, Taylor & Francis Group, New York, NY.

ASCE. (2009), "Report card for america's infrastructure", American Society of Civil Engineers, Reston, VA.

Decher, G. and Schlenoff, J.B. (2003), "Multilayer thin films", Wiley-VCH, Weinheim, Germany.

Dharap, P., Li, Z., Nagarajaiah, S. and Barrera, E.V. (2004), "Nanotube film based on single-wall carbon nanotubes for strain sensing", *Nanotechnology*, **15**(3), 379-382.

Hess, P.E. "Structural health monitoring for high-speed naval ships", *Proceedings of the 6th International Workshop on Structural Health Monitoring*, Stanford, CA, 3-15.

Holder, D.S. (2005), Electrical Impedance Tomography - Methods, History and Applications, Institue of Physics Publishing, Bristol, UK.

Hou, T.C., Loh, K.J. and Lynch, J.P. (2007), "Spatial conductivity mapping of carbon nanotube composite thin films by electrical impedance tomography for sensing applications", *Nanotechnology*, **18**(31), 315501.

Iijima, S. (1991), "Helical microtubules of graphitic carbon", *Nature*, **354**(6348), 56-58.

Loh, K.J. and Chang, D. (2010), "Zinc oxide nanoparticle-polymeric thin films for dynamic strain sensing", *J. Mater. Sci*., Online First, 1-10.

Loh, K.J., Hou, T.C., Lynch, J.P. and Kotov, N.A. (2009a), "Carbon nanotube sensing skins for spatial strain and impact damage identification", *J. Nondestruct. Eval*., **28**(1), 9-25.

Loh, K.J., Kim, J., Lynch, J.P., Kam, N.W.S. and Kotov, N.A. (2007), "Multifunctional layer-by-layer carbon nanotube-polyelectrolyte thin films for strain and corrosion sensing", *Smart Mater. Struct*., **16**(2), 429-438.

Loh, K.J., Lynch, J.P., Shim, B.S. and Kotov, N. (2008), "Tailoring piezoresistive sensitivity of multilayer carbon nanotube composite strain sensors", *J. Intel. Mat. Syst. Struct*., **19**(7), 747-764.

Loh, K.J., Thouless, M.D. and Lynch, J.P. (2000b), "Enhancing the mechanical and fracture properties of nanocomposites using carbon nanotubes", *Proceedings of the12th International Conference on Fracture*, Ottawa, Canada.

Mamedov, A.A., Kotov, N.A., Prato, M., Guldi, D., Wicksted, J. and Hirsch, A. (2002), "Molecular design of strong SWNT/polyelectrolyte multilayers composites", *Nat. Mater*., **1**(3), 190-194.

Mascarenas, D.L., Todd, M.D., Park, G. and Farrar, C.R. (2007), "Development of an impedance-based wireless sensor node for structural health monitoring", *Smart Mater. Struct*., **16**(6), 2137-2145.

Melloy, B.J., Harris, J.M. and Gramopadhye, A.K. (2000), "Predicting the accuracy of visual search performance in the structural inspection of aircraft", *Int. J. Ind. Ergonom*., **26**(2), 277-283.

Moore, M., Phares, B., Graybeal, B., Rolander, D. and Washer, G. (2001), "Reliability of visual inspection for highway bridges", FHWA-RD-01-020, Federal Highway Administration, Washington D.C.

Nagayama, K. (1997), "Self-assembly: naturés way to do it.", Royal Institution Discourses Series, Vega Science Trust, London, England.

Park, G., Sohn, H., Farrar, C.R. and Inman, D.J. (2003), "Overview of piezoelectric impedance-based health monitoring and path forward", *Shock Vib*., **35**(6), 451-463.

Park, S., Park, S.K., Shin, H.H. and Yun, C.B. (2009), "Wireless sensor self-diagnosis for piezoelectric actuating/ sensing networks", *Proceedings of the SPIE - The International Society for Optical Engineering*, San Diego, CA, 72920B.

Park, S., Yun, C.B., Roh, Y. and Lee, J.J. (2006), "PZT-based active damage detection techniques for steel bridge components", *Smart Mater. Struct*., **15**(4), 957-966.

Peairs, D.M., Park, G. and Inman, D.J. (2004), "Improving accessibility of the impedance-based structural health monitoring method", *J. Intel. Mat. Syst. Struct*., **15**(2), 129-139.

Rolander, D.D., Phares, B.M., Graybeal, B.A., Moore, M.E. and Washer, G.A. (2001), "Highway bridge inspection: state-of-the-practice survey", *Transport. Res. Record*, **1749**(1), 73-81.

Sohn, H. and Kim, S.B. (2010), "Development of dual PZT transducers for reference-free crack detection in thin plate structures", *IEEE T. Ultrason. Ferr*., **57**(1), 229-240.

Wilkinson, J.D. and Shaw, S. (1998), Dermatology, Churchill Livingston, Edinburgh, UK.

Yonemoto, N. and Shida, K. (1998), "Multi-functional sensing for high-sensitivity detection of initial state of iron rust", *Proceedings of the IEEE Instrumentation and Measurement Technology Conference*, St. Paul, MN, 1145-1148.